



Supplement of

A series of climate oscillations around 8.2 ka revealed through multi-proxy speleothem records from North China

Pengzhen Duan et al.

Correspondence to: Hanying Li (hanyingli@xjtu.edu.cn) and Hai Cheng (cheng021@xjtu.edu.cn)

The copyright of individual parts of the supplement might differ from the article licence.

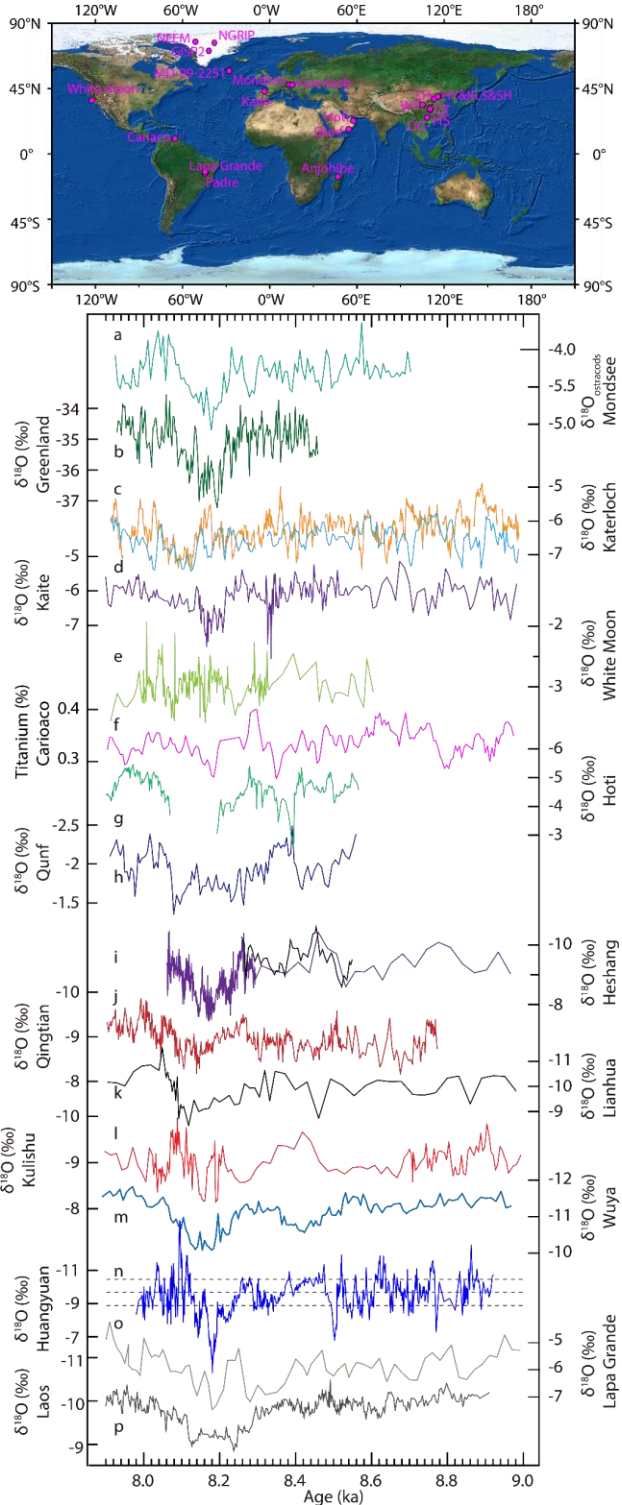


Figure S1. Comparison between speleothem BH-2 $\delta^{18}\text{O}$ and other records during 9.0–7.9 ka BP. The black dots in the world map represent the proxy locations mentioned in our main text. (a) $\delta^{18}\text{O}_{\text{ostracods}}$ record from Mondsee, Austria (Andersen et al., 2017). (b) Composite $\delta^{18}\text{O}$ record from Greenland ice core (Thomas et al., 2007). (c) $\delta^{18}\text{O}$ records (blue: K1, yellow: K3) from Katerloch cave, Austria (Boch et al., 2009). (d) $\delta^{18}\text{O}$ record of speleothem LV5

from Kaite cave, Spain (Domínguez-Villar et al., 2009). (e) Speleothem $\delta^{18}\text{O}$ record from White Moon cave, California, America (Oster et al., 2017). (f) Bulk Titanium content of Cariaco Basin sediments from ODP Site 1002 (Huag et al., 2002). (g) Speleothem $\delta^{18}\text{O}$ record from Hoti cave, Oman (Cheng et al., 2009). (h) High-resolution $\delta^{18}\text{O}$ record from Qunf cave, Oman (Fleitmann et al., 2003; Cheng et al., 2009) based on more precise ^{230}Th dating results (Cheng et al., 2009). (i–n) Asian monsoon speleothem $\delta^{18}\text{O}$ records from Heshang cave (Liu et al., 2013; Hu et al., 2008), Qingtian cave (Liu et al., 2015), Lianhua cave (Dong et al., 2018), Kulishu cave (Duan W et al., 2021), Wuya cave (Tan et al., 2020), and Huangyuan cave (this study). The horizontal blue and purple dashed lines in the Huangyuan cave record represent its mean and $\pm 1\sigma$ values, respectively. (o) Speleothem $\delta^{18}\text{O}$ record from Lapa Grande cave, Brazil (Stríkis et al., 2011). (p) Speleothem $\delta^{18}\text{O}$ record from TDM cave, Northern Laos (Wood et al., 2023). The speleothem $\delta^{18}\text{O}$ scales in c, d, and o are inverse to other speleothem records.

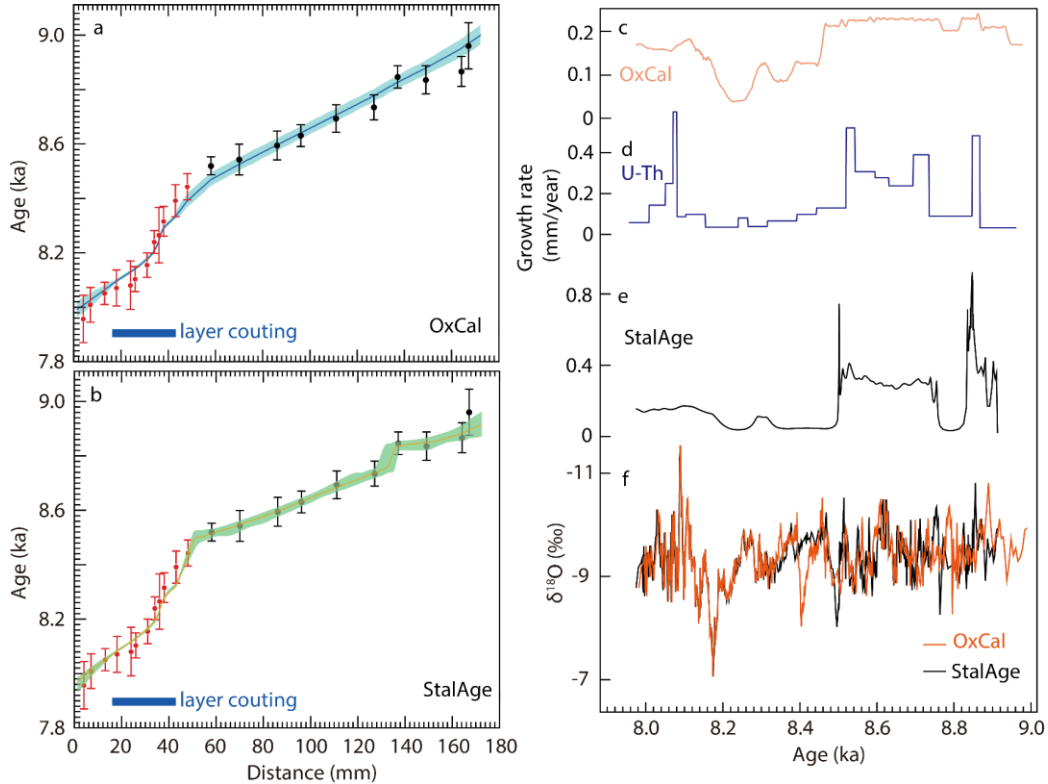


Figure S2. Estimation of age model. Subpanels (a) and (b) are reconstructed distance-chronology relationships using OxCal (Ramsey et al., 2008) and StalAge (Scholz and Hoffmann, 2011) algorithm, respectively. The blue and green shadings represent 95 % confidence interval. Error bars on ^{230}Th dates represent 2σ analytical errors. The red dates indicate the published results in Duan et al. (2023). The horizontal blue bar marks the range with layer counting. As can be seen, some U-Th dates are out of the confidence interval of modelled chronology in the OxCal results, which phenomenon doesn't occur in the StalAge model. This could suggest that the StalAge algorithm could be more reasonable for this study. (c–e) are established growth rate records using OxCal age model, U-Th dates and StalAge age model. The growth rate record using StalAge model is more consistent with the result directly based on U-Th dates, and more variable relative to the OxCal result which is rather smoothed. To sum up, we adopt the StalAge age model to reconstruct the chronology of speleothem BH-2. (f) marks the difference of $\delta^{18}\text{O}$ records using OxCal and StalAge reconstructed chronology. The offset of two records mainly occurs before 8.32 ka BP and almost disappears afterward.

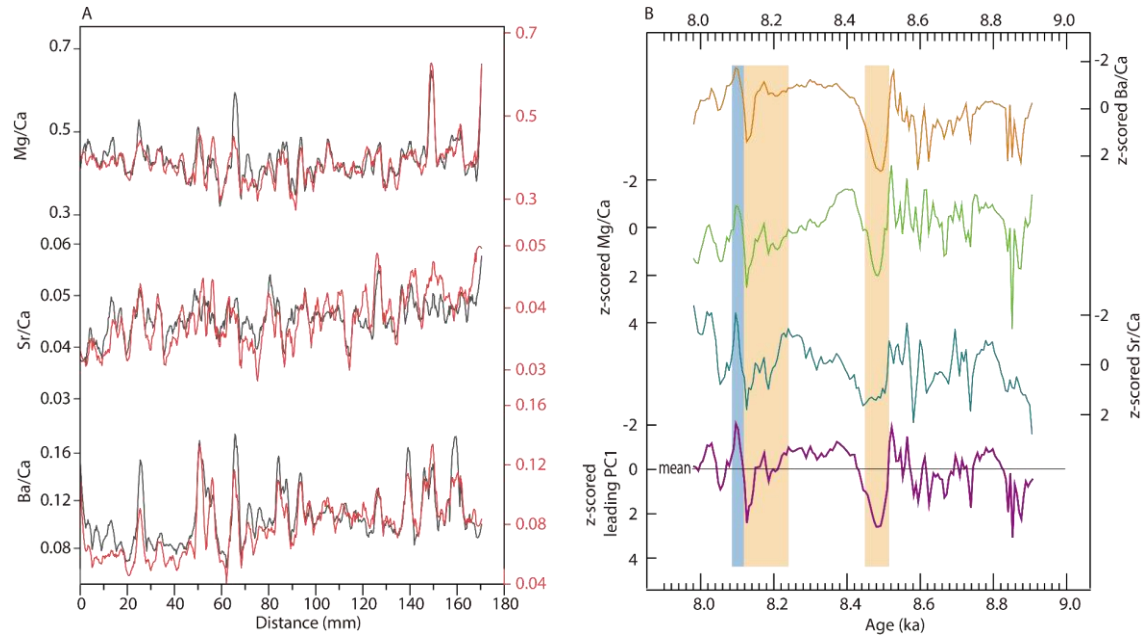


Figure S3. Replication of trace element ratios measurement and 30-year loess filtered z-scored results. (A) Replication test of two-time measurements for trace element ratios. As can be seen, despite the discrepancy of absolute values, the two-time results are broadly consistent, suggesting the robustness of LIBS technique. (B) Ba/Ca, Mg/Ca, Sr/Ca, and their leading PC1 records. The mean value of the PC1 record is indicated by the horizontal black line. The vertical yellow bars in the right subpanel mark the anomalously positive episodes and the light blue bar indicates the subsequent $\delta^{18}\text{O}$ overshoot after the 8.2 ka event same as the Figure 2.

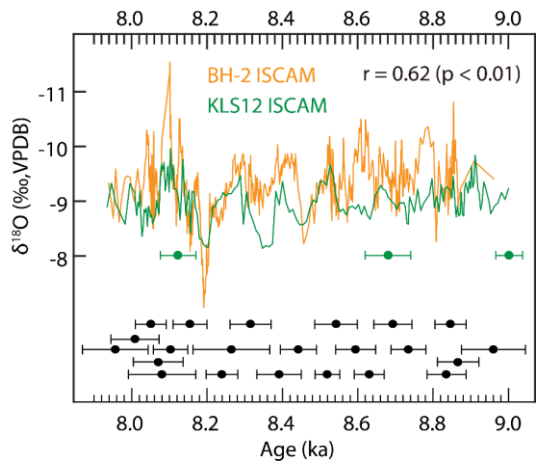


Figure S4. Replication test. ISCAM age model was used to reconstruct speleothems BH-2 (orange) and KLS12 (green) (Duan W et al., 2021) chronologies and $\delta^{18}\text{O}$ records. The correlation coefficient (r) between them is 0.62 at 99 % confidence level in their contemporary growth period. The ^{230}Th dates with 2σ analytical errors (green for KLS12 and black for BH-2) are presented for each speleothem record.

Table S1. ^{230}Th dating results for the BH-2. The error is at 2σ level.

Sample Number	depth (mm)	^{238}U (ppb)	^{232}Th (ppt)	$^{230}\text{Th} / ^{232}\text{Th}$ (atomic $\times 10^{-6}$)	$\delta^{234}\text{U}^*$ (measured)	$^{230}\text{Th} / ^{238}\text{U}$ (activity)	^{230}Th Age (yr) (uncorrected)	^{230}Th Age (yr BP)*** (corrected)	$\delta^{234}\text{U}_{\text{Initial}}^{**}$ (corrected)
BH-2-1(1)	4	111.7 ± 0.1	373 ± 8	544 ± 12	537.0 ± 2.4	0.1102 ± 0.0010	8080 ± 75	7956 ± 87	549 ± 2
BH-2-T	7	90.6 ± 0.1	322 ± 6	513 ± 11	531.0 ± 1.8	0.1105 ± 0.0006	8134 ± 43	8008 ± 64	543 ± 2
BH-2-2	13	110.9 ± 0.2	103 ± 3	1970 ± 60	542.7 ± 3.1	0.1113 ± 0.0012	8130 ± 38	8050 ± 41	555 ± 3
BH-2-2(1)	18	114.2 ± 0.1	164 ± 3	1293 ± 30	535.1 ± 2.9	0.1128 ± 0.0009	8158 ± 65	8070 ± 66	548 ± 3
BH-2-3	24	125.1 ± 0.1	117 ± 3	1961 ± 59	535.9 ± 2.0	0.1113 ± 0.0006	8160 ± 45	8080 ± 89	549 ± 2
BH-2-3a	26	103.6 ± 0.2	86 ± 2	2210 ± 49	530.8 ± 2.1	0.1112 ± 0.0006	8181 ± 44	8103 ± 46	543 ± 2
BH-2-4	31	122.4 ± 0.2	54 ± 2	4158 ± 92	527.2 ± 2.5	0.1118 ± 0.0006	8234 ± 44	8154 ± 45	540 ± 3
BH-2-4a	34	121.8 ± 0.2	90 ± 2	2492 ± 55	523.4 ± 2.2	0.1123 ± 0.0005	8315 ± 41	8239 ± 42	536 ± 2
BH-2-4b	36	99.2 ± 0.1	225 ± 13	828 ± 49	528.3 ± 2.2	0.1138 ± 0.0014	8400 ± 98	8264 ± 102	541 ± 2
BH-2-5	38	102.4 ± 0.1	213 ± 4	905 ± 19	527.1 ± 2.5	0.1142 ± 0.0006	8416 ± 47	8315 ± 55	540 ± 3
BH-2-6	45	111.8 ± 0.2	290 ± 6	735.8 ± 16	534.7 ± 2.6	0.1159 ± 0.0005	8503 ± 57	8391 ± 59	548 ± 2
BH-2-7	48	121.8 ± 0.2	57 ± 2	3220 ± 70	539.4 ± 2.0	0.1166 ± 0.0011	8513 ± 88	8442 ± 48	554 ± 3
BH-7a	58	134.5 ± 0.2	61 ± 1	4272 ± 94	538.1 ± 1.9	0.1170 ± 0.0004	8589 ± 32	8519 ± 33	551 ± 2
BH-2-8	70	140.8 ± 0.2	357 ± 7	765 ± 16	536.6 ± 2.8	0.1177 ± 0.0006	8651 ± 46	8542 ± 57	550 ± 3
BH-2-9	86	128.7 ± 0.2	85 ± 2	2942 ± 70	533.4 ± 2.3	0.1177 ± 0.0007	8668 ± 52	8594 ± 53	547 ± 2
BH-9a	96	117.5 ± 0.2	82 ± 2	2781 ± 61	533.0 ± 2.1	0.1181 ± 0.0005	8705 ± 39	8630 ± 40	546 ± 2
BH-2-10	111	135.9 ± 0.2	66 ± 2	4031 ± 101	529.5 ± 2.6	0.1186 ± 0.0006	8765 ± 51	8693 ± 51	543 ± 3
BH-2-11	127	151.4 ± 0.2	95 ± 2	3109 ± 70	525.3 ± 2.0	0.1189 ± 0.0006	8808 ± 45	8734 ± 46	538 ± 2
BH-2-11a	137	139.7 ± 0.2	97 ± 2	2863 ± 63	532.9 ± 2.2	0.1209 ± 0.0005	8921 ± 40	8846 ± 41	546 ± 2
BH-2-12	149	137.2 ± 0.2	74 ± 2	3657 ± 89	522.4 ± 2.6	0.1199 ± 0.0006	8907 ± 52	8835 ± 52	536 ± 3
BH-2-13	164	151.0 ± 0.2	178 ± 4	1696 ± 37	531.5 ± 2.4	0.1212 ± 0.0007	8950 ± 53	8866 ± 55	545 ± 2
BH-2-14	167	138.9 ± 0.2	120 ± 3	2345 ± 63	537.8 ± 2.8	0.1229 ± 0.0011	9039 ± 84	8960 ± 85	552 ± 3

U decay constants: $\lambda_{238} = 1.55125 \times 10^{-10}$ and $\lambda_{234} = 2.82206 \times 10^{-6}$. Th decay constant: $\lambda_{230} = 9.1705 \times 10^{-6}$.

* $\lambda^{234}\text{U} = ([^{234}\text{U}/^{238}\text{U}] \text{ activity} - 1) \times 1000$. ** $\delta^{234}\text{U}_{\text{initial}}$ was calculated based on ^{230}Th age (T), i.e., $\lambda^{234}\text{U}_{\text{initial}} = \lambda^{234}\text{U}_{\text{measured}} \times e^{\lambda^{234}\text{U} T}$.

Corrected ^{230}Th ages assume the initial $^{230}\text{Th}/^{232}\text{Th}$ atomic ratio of $4.4 \pm 2.2 \times 10^{-6}$. Those are the values for a material at secular

equilibrium, with the bulk earth $^{232}\text{Th}/^{238}\text{U}$ value of 3.8. The errors are arbitrarily assumed to be 50 %.

***B.P. stands for “Before Present” where the “Present” is defined as the year 1950 A.D..

References

- Andersen, N., Lauterbach, S., Erlenkeuser, H., Danielopol, D. L., Namotko, T., and Hüls, M.: Evidence for higher-than-average air temperatures after the 8.2 ka event provided by a Central European $\delta^{18}\text{O}$ record, *Quat. Sci. Rev.*, 172, 96–108, <http://dx.doi.org/10.1016/j.quascirev.2017.08.001>, 2017.
- Boch, R., Spötl, C., and Kramers, J.: High-resolution isotope records of early Holocene rapid climate change from two coeval stalagmites of Katerloch Cave, Austria, *Quat. Sci. Rev.*, 28, 2527–2538, <https://doi.org/10.1016/j.quascirev.2009.05.015>, 2009.
- Cheng, H., Edwards, R. L., Shen, C. C., Polyak, V. J., Asmerom, Y., and Woodhead, J.: Improvements in ^{230}Th dating, ^{230}Th and ^{234}U half-life values, and U-Th isotopic measurements by multi-collector inductively coupled plasma mass spectrometry, *Earth Planet Sci Lett*, 371–372, 82–91, <https://doi.org/10.1016/j.epsl.2013.04.006>, 2013.
- Cheng, H., Fleitmann, D., Edwards, R. L., Wang, X., Cruz, F. W., and Auler, A. S.: Timing and structure of the 8.2 kyr B.P. event inferred from $\delta^{18}\text{O}$ records of stalagmites from China, Oman, and Brazil, *Geology*, 37, 1007–1010, <https://doi.org/10.1130/G30126A.1>, 2009.
- Domínguez-Villar, D., Fairchild, I. J., Baker, A., Wang, X., Edwards, R. L., and Cheng, H.: Oxygen isotope precipitation anomaly in the North Atlantic region during the 8.2 ka event, *Geology*, 37, 1095–1098, <https://doi.org/10.1130/G30393A.1>, 2009.
- Dong, J., Shen, C. C., Kong, X., Wu, C. C., Hu, H. M., Ren, H., and Wang, Y.: Rapid retreat of the East Asian summer monsoon in the middle Holocene and a millennial weak monsoon interval at 9 ka in northern China, *J. Asian Earth. Sci.*, 151, 31–39, <https://doi.org/10.1016/j.jseas.2017.10.016>, 2018.
- Duan, P., Li, H., Sinha, A., Voarintsoa, N. R. G., Kathayat, G., Hu, P., and Cheng, H.: The timing and structure of the 8.2 ka event revealed through high-resolution speleothem records from northwestern Madagascar, *Quat. Sci. Rev.*, 268, 107104, <https://doi.org/10.1016/j.quascirev.2021.107104>, 2021.
- Duan, W., Ma, Z., Tan, M., Cheng, H., Edwards, R. L., and Wen, X.: Timing and structure of early-Holocene climate anomalies inferred from north Chinese stalagmite records, *Holocene*, 31, 1777–1785, <https://doi.org/10.1177/09596836211033218>, 2021.
- Fleitmann, D., Burns, S. J., Mudelsee, M., Neff, U., Kramers, J., Mangini, A., and Matter, A.: Holocene forcing of the Indian monsoon recorded in a stalagmite from southern Oman, *Science*, 300, 1737–1739, <https://doi.org/10.1126/science.1083130>, 2003.
- Hu, C., Henderson, G. M., Huang, J., Xie, S., Sun, Y., and Johnson, K. R. Quantification of Holocene Asian monsoon rainfall from spatially separated cave records, *Earth Planet. Sci. Lett.*, 266, 221–232, <https://doi.org/10.1016/j.epsl.2007.10.015>, 2008.
- Kobashi, T., Menziel, L., Jeltsch-Thömmes, A., Vinther, B. M., Box, J. E., and Muscheler, R.: Volcanic influence on centennial to millennial Holocene Greenland temperature change, *Sci. Rep.*, 7, 1–10, <https://doi.org/10.1038/s41598-017-01451-7>, 2017.
- Liu, D., Wang, Y., Cheng, H., Edwards, R. L., and Kong, X.: Cyclic changes of Asian monsoon intensity during the early mid-Holocene from annually-laminated stalagmites, central China, *Quat. Sci. Rev.*, 121, 1–10, <https://doi.org/10.1016/j.quascirev.2015.05.003>, 2015.

- Liu, Y. H., Henderson, G. M., Hu, C. Y., Mason, A. J., Charnley, N., and Johnson, K. R.: Links between the East Asian monsoon and north Atlantic climate during the 8,200 year event, *Nat. Geosci.*, 6, 117–120, <https://doi.org/10.1038/ngeo1708>, 2013.
- Oster, J. L., Sharp, W. D., Covey, A. K., Gibson, J., Rogers, B., and Mix, H. Climate response to the 8.2 ka event in coastal California, *Sci. Rep.*, 7, 1–9, <https://doi.org/10.1038/s41598-017-04215-5>, 2017.
- Ramsey, C. B.: Deposition models for chronological records, *Quat. Sci. Rev.*, 27, 42–60, <https://doi.org/10.1016/j.quascirev.2007.01.019>, 2008.
- Scholz, D., and Hoffmann, D. L.: StalAge—An algorithm designed for construction of speleothem age models. *Quat. Geochronol.*, 6, 369–382, <https://doi.org/10.1016/j.quageo.2011.02.002>, 2011.
- Stríkis, N. M., Cruz, F. W., Cheng, H., Karmann, I., Edwards, R. L., and Vuille, M. Abrupt variations in South American monsoon rainfall during the Holocene based on a speleothem record from central-eastern Brazil, *Geology*, 39, 1075–1078, <https://doi.org/10.1130/G32098.1>, 2011.
- Tan, L., Li, Y., Wang, X., Cai, Y., Lin, F., Cheng, H., Ma, L., Sinha, A., and Edwards, R. L. Holocene monsoon change and abrupt events on the western Chinese Loess Plateau as revealed by accurately dated stalagmites, *Geophys. Res. Lett.*, 47, e2020GL090273, <https://doi.org/10.1029/2020GL090273>, 2020.
- Thomas, E. R., Wolff, E. W., Mulvaney, R., Steffensen, J. P., Johnsen, S. J., and Arrowsmith, C. The 8.2 ka event from Greenland ice cores, *Quat. Sci. Rev.*, 26, 70–81, <https://doi.org/10.1016/j.quascirev.2006.07.017>, 2007.
- Wood, C. T., Johnson, K. R., Lewis, L. E., Wright, K., Wang, J. K., and Borsato, A.: High-resolution, multiproxy speleothem record of the 8.2 ka event from Mainland Southeast Asia. *Paleoceanogr Paleocl.*, 38, e2023PA004675, <https://doi.org/10.1029/2023PA004675>, 2023.